The Response of a Spherical Tissue-Equivalent Proportional Counter To ^{56}Fe Particles from 200-1000 MeV/nucleon.

B. B. Gersey[1)], T. B. Borak[1)], S. B. Guetersloh[1)], C. Zeitlin[2)], J. Miller[2)], L. Heilbronn[2)], T. Murakami[3)], Y. Iwata[3)]

1) Department of Radiological Health Sciences, Colorado State University, Fort Collins, Colorado 80523

2) Lawrence Berkeley National Laboratory, Berkeley, California 94720

3) Division of Accelerator Physics and Engineering, National Institute of Radiological Sciences, 9-1 Anagawa 4-chome, Inage-ku, Chiba 263, Japan

Abstract

The radiation environment aboard the space shuttle and the International Space Station includes high-Z and high-energy (HZE) particles that are part of the galactic cosmic radiation (GCR) spectrum. ^{56}Fe is considered to be one of the most biologically important parts of the GCR spectrum. Tissue-equivalent proportional counters (TEPC) are used as active dosimeters on manned space flights. These TEPC's are further used to determine average quality factor for each space mission. A TEPC simulating a 1-μm diameter sphere of tissue was exposed as part of a particle spectrometer to ^{56}Fe at energies from 200-1000 MeV/nucleon. The response of TEPC in terms of mean lineal energy $\overline{y}_F$, and dose mean lineal energy, $\overline{y}_D$, as well as energy deposited at different impact parameters through detector was determined for six different incident energies of ^{56}Fe in this energy range. Calculations determined that charged particle equilibrium was achieved for each of the six experiments. Energy depositions at different impact parameters were calculated using a radial dose distribution model and the results compared to experimental data.

I. Introduction

It has been estimated that during a three-year mission to Mars, an astronaut would receive a radiation dose equivalent of 1 Sv (1). During space travel outside the geomagnetosphere, the main source of chronic radiation exposure is from galactic cosmic radiation (GCR). Approximately 87% of the particles in the GCR spectrum are protons, 12% are helium nuclei and 1% are particles heavier than helium, often referred to as high-Z and high-energy (HZE) particles. The heaviest biologically important of these HZE particles is iron because of its relatively large contribution to radiation dose and together with the high LET (1,2).

Currently, tissue equivalent proportional counters (TEPC) are flown aboard the Space Shuttle and International Space Station as area monitors to characterize the radiation field inside the spacecraft (3,4,5). Energy deposition spectra produced by a TEPC can be used to calculate absorbed dose and estimate the average quality of radiation during the mission (6). In the past, it has been assumed that lineal energy, y, is numerically equivalent to LET. The measured distribution f(y) was assumed to be a direct measurement of the LET distribution, f(L), of the incident particles. However, recent comparisons of measurements of f(y) with a TEPC and f(L) using a particle spectrometer indicate that there are serious differences between the two distribution (7). This can cause large uncertainties in the corresponding estimates of quality factor. The objectives of this work were to carefully measure the response of a TEPC to ^{56}Fe particles for a range of energies across the (broad) peak of the GCR fluence vs. energy spectrum.

Previous measurements of TEPC response have used particle accelerators to produce HZE radiation of energies similar to those found in the GCR spectrum. Table I summarizes these experiments. Luxton and Fessenden (8) irradiated a 12.7-mm diameter TEPC with a 2.5-mm tissue equivalent (TE) wall. This TEPC simulated a 2-μm diameter sphere of tissue using a TE gas at a pressure of 67 torr in the active chamber volume. This series of experiments found values for the dose-averaged lineal energy of carbon, helium and neon at initial energies of 400 MeV/nucleon, 230 MeV/nucleon and 400 MeV/nucleon respectively. Dose-averaged lineal energy values were also taken for these three particle beams as each beam was modified with a variable thickness water column. Metting et al. (9) determined energy deposition in a wall-less microdosimeter as a function of impact parameter for 600 MeV/ nucleon ^{56}Fe particles. Positions of the ^{56}Fe particles were obtained using one pair of silicon position sensitive detectors (PSDs) to measure X and Y of the incident ion. An experiment performed by Rademacher et al. (10) used a solid walled 12.7-mm diameter TEPC that was exposed to 1.05 GeV/ nucleon ^{56}Fe particles. The detector response as a function of impact parameter was measured using two X-Y pairs of PSDs (one upstream and one downstream of the TEPC).

In the present series of experiments, data were obtained at ground based accelerator facilities that produced beams of ^{56}Fe with kinetic energies between 200 and 1000 MeV/nucleon ($\beta = v/c = 0.56 – 0.88$). Specifically, a spherical TEPC was exposed to ^{56}Fe beams at energies spanning the peak of the GCR Fe spectrum. In each case a particle spectrometer measured the charge and position of each incident particle both upstream and downstream of the TEPC. With this experimental arrangement, the trajectory of the particle through the TEPC could be reconstructed and related to the energy deposition recorded by the detector. Frequency distributions of energy deposition (i.e., response functions) were determined for uniformly incident beams of Fe, and these distributions were used to compute absorbed dose as well as average values of lineal energy, y.

II. Materials and Methods

Six experiments were performed, four with the Alternating Gradient Synchrotron (AGS) at Brookhaven National Laboratory in Upton, NY, and two at the Heavy Ion Medical Accelerator (HIMAC) at the National Institute of Radiological Sciences in Chiba, Japan. Features of the six experiments are summarized in Table II. For each experiment, calculations were performed to determine the energy of the Fe particles after passing through the vacuum window, and through the experimental apparatus upstream of the TEPC. During the experiment BNL97_2, 8.2-cm of polyethylene was placed in the particle beam upstream of all experimental apparatus to reduce the energy of the primary beam. During the BNL98 experiment, this procedure was repeated with 12.5-cm of polyethylene in the beam.

The same spherical TEPC[1] was used in all six experiments. The TEPC had an active volume 12.7-mm in diameter and a tissue equivalent wall 2.54-mm thick. The active volume was filled with a propane-based tissue equivalent gas at a pressure of 33 torr, simulating a sphere of tissue having a diameter of 1-μm. Calibration was accomplished using an internally mounted ^{244}Cm alpha particle source that was mounted with a gravity-controlled gate. When the TEPC was inverted from its operational orientation, the gate opened and alpha particles emanating from the source deposited 84.15 keV in the TEPC gas cavity.

In each of the six experiments, the energy signal from the TEPC was sent to an EG&G Ortec[2] charge sensitive preamplifier, the output of which went to two separate EG&G Ortec shaping amplifiers. The gains of the two shaping amplifiers were set so that the difference in amplification was approximately a factor of 12.

[1] Far West Technologies, Inc. Goleta, CA.

[2] EG&G Ortec, Oak Ridge, TN

The TEPC was positioned within a particle spectrometer (Fig. 1) that measured individual particle events during the experiment. Four pairs of PSDs (denoted PSD1-PSD4 in Fig. 1) were used to track both the position and the energy of each particle as it passed through the apparatus. An individual PSD measured a single Cartesian coordinate (X or Y). Thus each pair determined the position of each particle in the transverse plane. The PSDs are lithium-drifted silicon detectors fabricated in the shape of circular disks, with radii of 20-mm and thickness between 800-μm and 1050 -μm. The total charge collected, Q, on one side of the detector, was proportional to the total amount of energy deposited in the PSD by the particle. On the other side of the detector, charge was divided between the top (q_1) and bottom (q_2) of a PSD (for the Y coordinate), or left (q_1) and right (q_2) of a PSD (for the X coordinate PSD). The amounts of charge collected in q_1 and q_2 can be related to the X or Y position of the incident particle (16). One X and one Y PSD were used in each PSD pair as seen in Fig. 1. One 3-mm thick lithium drifted silicon detector was placed downstream of the PSDs to provide additional energy deposition information for each particle.

The data acquisition system was triggered by a coincidence between the TEPC signal and one of the PSD signals upstream of the TEPC. Data was recorded on an event-by-event basis. For each experiment, data for a minimum of 2 million triggers were recorded. Iron ions can fragment into lighter ions as they pass through materials. The trigger threshold in the PSD was set so that only primary beam ions and fragments within a few charge units of the primary fired the trigger. For this analysis, energy deposition signals from PSDs both upstream and downstream of the TEPC were used to select events corresponding to the passage of Fe through the TEPC, thereby giving a clean sample of events.

III. Data Analysis

The two signals q_1 and q_2 produced by each PSD were related to either the X or the Y coordinate of the traversing particle. In certain regions of the PSDs, positions as calculated by the nominal method (16) are systematically in error; the errors are smallest near the center of the detectors and increase towards the edges. A calibration procedure was used to correct for these distortions, yielding improved accuracy in the position determination. A mask was fabricated, consisting of a thick (2.54 cm) brass plate with holes 0.8-mm in diameter drilled through it. The holes were spaced 6-mm apart in a radial pattern. During the experiments, dedicated data-taking runs were performed with the mask aligned with a PSD pair. The brass plate was thick enough to stop Fe particles, so that only particles passing through the holes were registered in the PSD[3]. The procedure was repeated for each PSD pair. The data were used to obtain a transformation from q_1 and q_2 into the corresponding position. This alignment was achieved by performing univariate multiple regressions on the PSD response data similar to the method described by Wong *et al.* (16) and Chapman (17).

The magnitude of the total-charge signal Q from each PSD was proportional to the amount of energy deposited in the PSD by the traversing particle. The energy deposition spectrum for each PSD has a prominent peak corresponding to the primary Fe, and distinct peaks corresponding to particles with charges less than that of the primary particles. Because the forward-going projectile fragments continue with velocities close to that of the incident beam, the energy deposition is approximately proportional to the square of the fragment charge. This information was used to select events where the incident Fe did not fragment in the TEPC.

In the data analysis, the X, Y and Z positions of a particle were defined relative to the center of the active volume of the TEPC, using information from PSD2. The Z axis is defined to be the primary beam direction; X and Y represented orthogonal coordinates in the transverse plane. The impact parameter is defined as the radial distance in millimeters from the center of the TEPC, so that particles traversing the

[3] This is an oversimplification. Light fragments formed in nuclear interactions in the brass mask can also reach the PSDs, but can be identified (and removed from the sample) in the analysis because the energy they deposit in the PSDs is inconsistent with that from an Fe ion that passes through a hole.

full diameter of the active volume of the TEPC had impact parameters near 0-mm. Particles that traversed the TEPC at the interface between the active volume and wall had impact parameters equal to 6.35-mm. Particle events that grazed the outside edge of the wall had impact parameters equal to 8.89-mm.

Electronic Noise

There was no attempt to actively suppress electronic noise in the TEPC and amplifiers. During each run random triggers were supplied to the data acquisition system. These events were easily recognized in the analysis as having an energy signal from the TEPC but with no energy deposited in the PSDs. The distribution of the TEPC signals on these events indicated that energy depositions below 3 keV cannot be distinguished from noise.

Many events that satisfied the Fe selection criteria in the PSDs had energy depositions below 3 keV in the TEPC. Virtually all of these events had impact parameters greater than 8.9-mm, which meant that they missed the TEPC altogether. Fig 2 shows the energy deposition distribution for these events. The primary graph in Fig. 2 is the complimentary cumulative distribution of events when the impact parameter was greater than 8.9-mm. The insert in Fig. 2 is a histogram (i.e. density distribution) of the number of these same events versus energy deposition in the TEPC. This Figure illustrates that there are occasional high-energy deposition events that occur at impact parameters greater than 8.9-mm. A comparison of the data found in Fig. 2 and the distribution of random-trigger events concluded that these two spectra were virtually identical. In both spectra, 99% of the events had energy deposition of less than 3 keV.

A scatter plot of energy deposition in the TEPC versus impact parameter for impact parameters greater than or equal to 8.9-mm is shown in Fig. 3. A chi-squared test of independence was performed on the events shown in Fig. 3. The chi-squared test was constructed to determine if there was a correlation between the energy deposited in the TEPC and the impact parameter of the event. The results of this test concluded that there was no statistical basis for any correlation between the energy deposited in the TEPC and the impact parameter of these events ($p = 0.62$). A chi-squared test of independence performed on events from the same experiment with impact parameters less than 8.9-mm showed that there was a strong dependence between energy deposited and impact parameter. ($p = 1x10^{-87}$). We conclude that the energy deposition in the TEPC by particle events with impact parameters greater than 8.9-mm were consistent with electronic noise. These events were therefore excluded from further analysis.

Formation of Uniform Incident Fluence

The fluence of Fe ions through the TEPC was not spatially uniform. In order to obtain the complete response of the TEPC for a uniform beam, the data for all incident Fe particles were separated into a grid with a resolution of 1-mm x 1-mm. The corresponding event size distributions for each grid were normalized to one incident particle and the spectra for each grid combined to form the response for uniformly incident Fe ions. This distribution is referred to as the response function for the spherical TEPC. The response function for a given experiment was used to obtain average values corresponding to absorbed dose, D, frequency averaged lineal energy, $\overline{y}_F$, and dose averaged lineal energy, $\overline{y}_D$.

Track Structure Model Calculations

A radial track structure model developed by Cucinotta et al. (18) was used to compute energy depositions in spherical volumes for comparison with the measured data. The output of this model was in the form of dose in water (Gy) at discrete radial distances from a HZE track. An example of the predictions of this model for ^{56}Fe at 360 MeV/nucleon is shown in Fig. 4. These dose distributions were then superimposed on a sphere simulating incident ^{56}Fe particles at different impact parameters. Energy deposited by the track for radii outside of the sphere was considered to have escaped the sensitive volume and was therefore not recorded, giving an estimate of the amount by which the measured LET was reduced due to delta rays escaping the volume of interest. The calculation was first performed assuming that the ^{56}Fe

particle was passing through a homogeneous medium. In a second calculation, a heterogeneous medium was simulated to take into account the wall of the spherical TEPC, which has a density approximately 14,000 times greater than the gas cavity. Thus it was possible to estimate the influence of delta rays entering the gas cavity from ionization of atoms in the high-density wall. This computation simulated only the radial extension of the track and did not take into account any forward transport of electrons as the ^{56}Fe particle passed through the high-density wall before entering the sensitive volume of the detector.

IV. Results

Figure 5 shows the distribution of energy deposited in the TEPC by 360 MeV/nucleon Fe particles with impact parameters of less than 0.5-mm, i.e., particles passing through the center of the detector. The path length of particles through the active volume of the TEPC changes by less than 2% as the impact parameter of the particle goes from 0-mm to 1-mm. Since the estimated uncertainty in the position measurement of the particles was less than 0.5-mm, the particle path lengths through the detector for events in this distribution were therefore known to within a 2% uncertainty. The mean of the distribution is 173 keV (FWHM 16%). The variance in the energy deposition in the main peak of this distribution is almost entirely attributable to variations due to energy-loss straggling and gas multiplication within the TEPC. The LET of a 360 MeV/nucleon ^{56}Fe ion is 214 keV/μm, so that on average only 81% of the energy transferred to the gas in the sensitive volume is actually deposited in the volume. The remainder is assumed to escape in the form of energetic delta rays. Similar results were observed for all incident energies and are summarized in Table III.

Figure 6 shows the complete response of the spherical TEPC for a uniformly incident beam of 360 MeV/nucleon Fe particles. There is a broad distribution of energy deposition, with a peak near 160 keV and a large number of events with very small energy depositions, continuing below 50 keV. As described earlier, these are significantly above the electronic noise (99% of which is below 3 keV), and the number of events does not correspond to the expected chord length distribution for a uniformly incident beam of particles incident upon a sphere (i.e., μ-randomness). There is also a long tail of events with very large energy depositions above 200 keV. Some of these events deposit more than twice the energy expected for a particle with this LET having the maximum trajectory through the sphere. Data from the other experiments showed that the shape of the response functions were similar for all energies.

In order to understand the shape of the response function, the energy deposition distribution was separated into three regions, A, B and C, as shown in Fig. 6. The X and Y coordinates of the incident particles in each region were plotted in a two dimensional histogram with the base of the histogram corresponding to the X-Y coordinate when Z = 0 (i.e. center of the sphere in the direction of the beam). The results for all three regions are shown in Fig. 7.

Events in region A are due to ions that pass through the center of the detector. Events in the broad peak from 50 to 200 keV correspond to particles passing through the sensitive volume of the TEPC (not shown). The small energy depositions in region B are from particles that pass through an annular area corresponding to the dimensions of the plastic wall of the TEPC. Electrons that originate in the wall and manage to penetrate into the sensitive volume cause these events. The very large energy depositions in region C also have an annular pattern, as well as a cluster of events along a line through the detector. The events in this annulus have a mean impact parameter that is very near the diameter of the sensitive volume. Thus when a Fe ion grazes the inside edge of the wall, a large number of soft delta rays penetrate into the sensitive volume and create a large pulse that resembles the passage of a very high LET particle through the gas volume. The events along the centerline are generated when the Fe particle passes through the sensitive volume and strikes the anode or grid wires. These wires are very thin (45-um) with high density (ρ = 7.8 g cm^{-3}). The resulting burst of electrons from the wire produces a large pulse comparable to that generated by the passage of a very high LET particle.

Energy deposition as a function of impact parameter was calculated for each ^{56}Fe beam energy. Figure 8 shows the results for 360 MeV/nucleon. The black circles correspond to the mean energy deposited for the corresponding trajectory. The combined uncertainty in the estimated impact parameter and mean energy deposition is on the order of the symbol size. The procedure for determining the mean energy deposited was similar to that used by Rademacher *et al*. (10). The solid black line represents a calculation where the energy deposition is given by (LET • chord length), where the chord length is a simple geometric function of impact parameter. In this calculation, energy deposition is maximal when the particle passes through the center of the sphere, and goes to zero when the impact parameter is equal to the radius of the sphere. For impact parameters near zero, the data show an average energy deposition that is about 20% less than this simple LET approximation. As impact parameter increases, the data show greater energy deposition than this calculation predicts, with a narrow peak just as the particle passes through the inside edge of the wall of the TEPC. Similar results were observed by Rademacher *et al.* for 1050 MeV/nucleon Fe (10).

The dashed gray line in Fig. 8 shows a calculation of energy deposition in a homogeneous medium using the radial track model of Cucinotta et al (18). The model predicts that for zero impact parameter, more than 50% of the energy transferred by the ^{56}Fe ion escapes the 1-μm diameter sphere; in strong contrast to the data, which show about 20% losses. This difference may be attributable to delta rays generated in the front wall of the detector that enter the sensitive volume and contribute to the measured energy distribution – the radial model does not include this forward component of electrons. If this is the case, it follows that the enhancement of delta rays from the forward wall does not fully compensate for the delta rays that escape the sensitive volume. Thus for these events, charged particle equilibrium is not achieved.

The solid gray line in Fig. 8 represents energy deposition using the radial dose model for the heterogeneous geometry that takes into account the difference in density between the gas and the wall that surrounds the gas cavity. The spatial density of electrons generated in the wall is much higher than that of electrons generated in the gas, but the radial dimensions of the track are also reduced. The results of the model are similar to the homogenous case for small impact parameters, but the heterogeneous model predicts an enhancement in energy deposition near the edge of the sensitive volume, similar to that seen in the data. This analysis was repeated for all energies and the results are summarized in Table III.

As shown above, charged particle equilibrium was not achieved for Fe particles passing through the center of the TEPC. The data were analyzed to determine if energy deposition integrated over the complete response function was sufficient to provide a correct estimate of absorbed dose. This analysis was performed by computing the LET, Λ, of a monoenergetic uniform fluence of particles, that would give the same dose as that recorded by integrating the response function to the TEPC. This calculation took into account the projected surface area of the complete detector (cavity plus wall) rather than just the cavity, since there were many recorded events from particles that missed the cavity but passed through the wall. If Λ was equal to LET then the TEPC provided an accurate estimate of absorbed dose. The results shown in Table III and Fig. 9 indicate that Λ was within 6% of the numerical LET.

The energy deposition patterns in a TEPC are related to the LET of the incident heavy ions in a very complicated way. Using a TEPC to estimate quality factors has always been a desirable feature when applied to radiation protection dosimetry. To investigate this, the response functions were converted into distributions of lineal energy and used to determine frequency averaged lineal energy, $\overline{y}_f$, and dose averaged lineal energy, $\overline{y}_D$. The results are shown in Table III and Fig. 9. For the ideal case where energy deposition is (LET • chord length), $\overline{y}_f$, should be identical to LET. It can be seen that for Fe at these energies, measured values of $\overline{y}_f$ are consistently lower than LET due to the escape of electrons from the sensitive volume. However, $\overline{y}_D$ is always within 8% of LET.

We have computed a quality factor using the known LET of the monoenergetic ^{56}Fe beams and data from the TEPC. In one case the quality factor, Q(L=y), was computed using the assumption that the distribution of LET was identical to the measured distribution f(y). In the second case, $Q(L=\overline{y}_D)$ was determined from only a single value of L assumed to be equal to $\overline{y}_D$ obtained from f(y). These results are shown in Fig. 10. For monoenergetic beams, Q(L=y) overestimated the true quality factor be as much as 20% whereas $Q(\overline{y}_D)$ was always within 4% of the true quality factor. The same computation was performed assuming a uniform mixture of ^{56}Fe particles at each of the six energies. For this case, Q(L=y) overestimated Q by 18% and $Q(\overline{y}_D)$ underestimated Q by 3%.

V. Conclusions

We have measured the response of a spherical tissue equivalent proportional counter to ^{56}Fe ion beams at several energies between 200 to 1000 MeV per nucleon. The experiments were performed at the AGS in Brookhaven National Laboratory in the US and at the HIMAC at the National Institute for Radiological Sciences in Japan. Particles were detected with a spectrometer that recorded the charge and position of each ion immediately upstream and downstream of the TEPC. Approximately 10^6 events were recorded for each experiment and analyzed off-line. The results reported here were for a uniform beam of Fe particles that entered and exited the detector without any charge-changing nuclear interactions. In all cases the gas pressure was regulated to simulate a sphere of tissue 1 μm in diameter.

The data at all energies indicated that track structure influences the pattern of energy deposition in the sensitive volume. For particles that pass through the center of the sphere, approximately 20% of the LET escapes the 1μm diameter volume. A model describing the radial distribution of the track indicated that over 50% of the LET should escape this volume. This difference between the data and model is attributed to delta rays produced in the front wall of the detector that have sufficient forward momentum to enter the gas cavity and contribute to energy deposition. However this delta ray enhancement from the forward wall is not sufficient to compensate for ionization electrons that escaped as the Fe particle passed through the sphere.

There is also a strong enhancement of events with very small energy depositions. These events originate from Fe particles that do not cross the sensitive volume but pass through the side-walls of the TEPC. Since the density of the wall is more than 10,000 times that of the gas cavity, there are many more electrons generated in the wall; however only a few of them have sufficient range to penetrate into the sensitive volume to produce a measurable energy deposition. Because the projected area of the wall is large, these events occur frequently and make a significant contribution to the response of the TEPC. These could easily be misinterpreted as incident particles with low LET.

When the trajectory of the Fe particle through the wall is very close to the inside boundary of the gas cavity, a large number of electrons enter the sensitive volume, producing a signal that resembles that produced by the passage of a high LET particle through the detector. Some of these events produce more that twice the energy deposited when the primary incident particle passes directly through center of the sensitive volume.

One other class of events is generated when the incident Fe particle strikes the anode or grid wires of the TEPC. Since the high-density wires are very thin, many delta rays can escape into the gas and produce a large pulse.

In spite of the complicated response function, the detector does give a reasonably good estimate of absorbed dose. There seems to be sufficient enhancement of energy deposition from delta rays produced in the wall to compensate for high-energy delta rays that escape the spherical volume. Thus while charged particle equilibrium is not preserved on an event-by-event basis, it is preserved when the detector

response is integrated over the complete response function that includes particles that do not pass through the sensitive volume.

A spherical TEPC does not make a direct measurement of LET for Fe particles at these energies and therefore such a TEPC should not be considered as an LET spectrometer. In the ideal case, the frequency-averaged lineal energy, $\overline{y}_f$, should be numerically equivalent to LET, but these data show that $\overline{y}_f$ is always significantly less than LET. However, dose averaged lineal energy, $\overline{y}_D$, does approximate LET. Computations of quality factor indicated that using the assumption that $\Phi(L)$ is identical to $f(y)$ yields a value that overestimates the true quality factor by 20%. The quality factor determined from the dose averaged value of y, $\overline{y}_D$ is always within 4% of the true value. It could be argued that since radiation risks are not always known with high precision either method might be suitable for estimating dose equivalent. It will be necessary to collect data for other ions in order to confirm this hypothesis.

VI. Acknowledgments

We gratefully acknowledge support for this research by the NASA Specialized Center of Research and Training in Radiation Health. Travel support was received from the National Science Foundation grant INT-9910062. Additional support came from the Research Project with Heavy Ions at National Institute of Radiological Sciences - HIMAC, Chiba, Japan. This work was supported at LBNL by the Space Radiation Health Program of the National Aeronautics and Space Administration under NASA Grant Numbers L14230C and H31909D, through the U.S. Department of Energy under Contract No. DE-AC03076SF00098. We would like to thank Dr. F.A. Cucinotta for permitting us to use his calculations for the radial distribution of dose for HZE particles.

VII. References

1. NCRP, Guidance on Radiation Received in Space Activities. Report 98, National Council on Radiation Protection and Measurements, Bethesda, MD, 1989.
2. NCRP, Radiation Protection Guidance for Activities in Low Earth Orbit. Report 132, National Council on Radiation Protection and Measurements, Bethesda, MD, 2000.
3. G.D. Badhwar, The Radiation Environment in Low-Earth Orbit. Radiat Res. 148, S3-S10 (1997).
4. G.D. Badhwar, F.A. Cucinotta, L.A. Braby, and A. Konradi, Measurements on the Shuttle of the LET Spectra of Galactic Cosmic Radiation and Comparison with the Radiation Transport Model. Radiat Res. 139, 344-351 (1994).
5. G.D. Badhwar, A. Konradi, A. Hardy, and L.A. Braby, Active Dosimetric Measurements On Shuttle Flights. Nucl. Tracks Radiat. Meas. 20, 13-20 (1992).
6. http://sragnt.jsc.nasa.gov/docs/TM104782/techmemo.htm
7. T. Doke, T. Hayashi, and T.B. Borak, Comparisons of LET Distributions Measured in Low Earth Orbit Using Tissue-Equivalent Proportional Counters and the Position Sensitive Si-Detector Telescope (RRMD-III). Accepted for publication Radiat Res. March (2001).
8. G. Luxton and P. Fessenden, Microdosimetric Measurements of Pretherapeutic Heavy Ion Beams. Radiat Res. 79, 256-272 (1979).
9. N.F. Metting, H.H. Rossi, L.A. Braby, P.J. Kliauga, J. Howard, M. Zaider, W.Schimmerling, M. Wong, and M. Rapkin, Microdosimetry near the Trajectory of High-Energy Heavy Ions. Radiat Res. 116, 183-195 (1988).
10. S.E. Rademacher, T.B. Borak, C. Zeitlin, L. Heilbronn, and J. Miller, Wall Effects Observed in Tissue-Equivalent Proportional Counters from 1.05 Gev/nucleon Iron-56 Particles. Radiat Res. 149, 387-395 (1998).
11. W. Glass and L. Braby, A Wall-Less Detector for Measuring Energy Deposition Spectra. Radiat Res. 39, 230-240 (1969).
12. R.C. Rodgers, J.F. Dicello, and W. Gross, The Biophysical Properties of 3.9-GeV Nitrogen Ions. Radiat Res. 54, 12-23 (1973).

13. P. Kliauga, R.D. Colvett, L.J. Goodman, and Y.M. Lam, Microdosimetry of 400 MeV/AMU ^{12}C and 450 MeV/AMU ^{40}Ar Beams. In Proceedings of the Sixth Symposium on Microdosimetry, (H.G. Ebert and J. Booz, Eds.), pp. 1173-1183. Harwood Academic Publishers Ltd., London, 1978.
14. J.F. Dicello, H.I. Amols, M. Zaider, and G. Tripard, A Comparison of Microdosimetric Measurements with Spherical Proportional Counters and Solid-State Detectors. Radiat Res. 82, 441-453 (1980).
15. J.F. Dicello, M. Wasiolek, Measured Microdosimetric Spectra of Energetic Ion Beams of Fe, Ar, Ne, and C: Limitations of LET Distributions and Quality Factors in Space Research and Radiation Effects. IEEE Trans. Nucl. Sci. 38, 1203-1209 (1991).
16. M. Wong, W. Schimmerling, M. H. Phillips, B. A. Ludewigt, D.A. Landis, J.T. Walton, and S.B. Curtis, The Multiple Coulomb Scattering of Very Heavy Charged Particles. Med. Phys. 17(2),163-171 (Mar/Apr 1990).
17. P.L. Chapman, "Applied Regression Methods." Applications of Probability and Statistics in Health Physics. Ed. T. Borak. Medical Physics Publishing, Madison.
18. F.A. Cucinotta, R. Katz, J. W. Wilson, R. R. Dubey, Heavy Ion Track-Structure Calculations for Radial Dose in Arbitrary Materials. NASA Technical Paper 3497 (February 1995).

DISCLAIMER

FIGURE CAPTIONS

FIG 1. The experimental apparatus, showing the position of the TEPC within the particle spectrometer.

FIG 2. Distribution of energy deposition in the TEPC by 200 MeV/u Fe particles with impact parameters greater than 8.9-mm. Density distribution of same events shown in insert.
FIG. 3. Scatter plot of energy deposition in the TEPC vs. impact parameter for 200 MeV/u iron particles with impact parameters greater than 8.9 mm.

FIG.4. The radial dose distribution from a 360 MeV/nucleon ^{56}Fe particle track in water as calculated by the radial dose model (17).

FIG.5. Distribution of energy deposited in the TEPC by 360 MeV/u Fe particles with impact parameters less than 0.5-mm.

FIG.6. Probability distribution of energy deposited in the TEPC by 360 MeV/u Fe particles with three regions of energy deposition highlighted (A,B,C).

FIG.7. Three-dimensional histograms of the three regions of energy deposition selected in Fig. 6. The X and Y-coordinates represent the particle location in the plane normal to the beam axis. Z-coordinates represent frequency of particle events.

FIG.8. Black filled circles: Mean energy deposited by 360 MeV/u Fe particles as a function of impact parameter. The line through the circles is to guide the eye. Dashed gray line: results of calculations performed using the radial dose model (17) assuming homogeneous conditions between the TEPC cavity and wall. Solid gray line: results of calculations performed using the radial dose model assuming heterogeneous conditions existing between the TEPC cavity and wall. Black line: results obtained by multiplying the LET of 360 MeV/u ^{56}Fe ions by the chord length through the detector volume at the given impact parameter.

FIG.9. LET, mean lineal energy, $\overline{y}_f$, dose mean lineal energy, $\overline{y}_D$, LET computation results, Λ, for Fe particles at 200,360,540,700,790,1000 MeV/u.

FIG.10. Bar graph showing true quality factor Q in black, results of calculations assuming $Q(L=\overline{y}_D)$ in gray, and results of calculations assuming $Q(L=y)$ in stripes for six energies of Fe.

Table I
Previous Experiments with HZE Particle Beams Using A TEPC

Reference	TEPC Type	Particle Species	Particle Beam Energy (MeV/nucleon)	Position and Particle Identification
Glass and Braby (11)	Spherical wall-less	He	1.125	None
Rodgers et al. (12)	Spherical walled,Spherical wall-less	N	3900	None
Kliauga et al. (13)	Spherical wall-less	C, Ar	400, 450	None
Luxton and Fessenden (8)	Spherical walled	He, C, Ne	230, 400, 400	None
Dicello et al. (14)	Spherical walled	π^-	167	None
Metting et al. (9)	Cylindrical wall-less	Fe	600	One dimensional positional and species determination by PSD
Dicello and Wasiolek (15)	Spherical walled, cylindrical wall-less	Fe, Ar, Ne, C	535, 570, 557, 400	None
Rademacher et al. (10)	Spherical walled	Fe	1050	Two dimensional positional and species determination by PSD's

Table II
Properties of the ^{56}Fe Beams Used in the Experiments.

Experiment Name	*Extracted Beam Energy (MeV/nucleon)*	*Energy at Entrance to TEPC Gas Cavity (MeV/nucleon)*	*Velocity of ^{56}Fe (β)*	*Maximum Energy of Electron Ejected From ^{56}Fe Track (MeV)*
HIMAC00	250	200	0.57	0.48
HIMAC99	400	360	0.69	0.93
BNL97_1	600	540	0.77	1.51
BNL98	1087	700	0.82	2.09
BNL97_2	1087	790	0.84	2.44
BNL99	1087	1000	0.87	3.33

Table III

Summary of Data and Model Calculations for ^{56}Fe.

^{56}Fe Beam Energy (MeV/nucleon)	**LET of ^{56}Fe Particles**	**Mean (FWHM), Data**	**Mean, Model**	**$\overline{y}_f$**	**$\overline{y}_D$**	**Λ**
200	302	254 (35)	148	199	328	309
360	214	173 (28)	101	146	216	227
540	179	136 (24)	83	134	173	178
700	163	127 (19)	74	125	159	N/A
790	157	117 (13)	71	118	153	N/A
1000	149	116 (12)	65	106	147	154

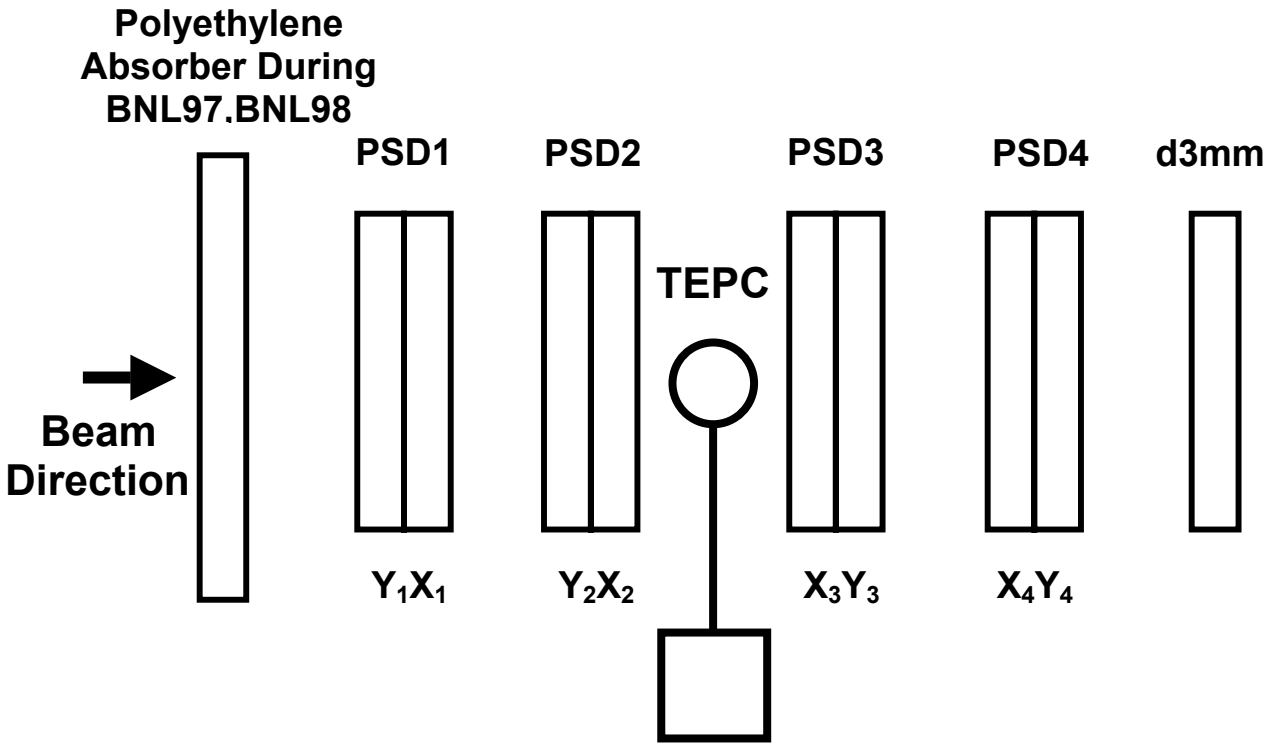
Polyethylene
Absorber During
BNL97.BNL98
PSD1
PSD2
PSD3
PSD4
d3mm
TEPC
Beam
Direction
Y1X1
Y2X2
X3Y3
X4Y4

Figure 1

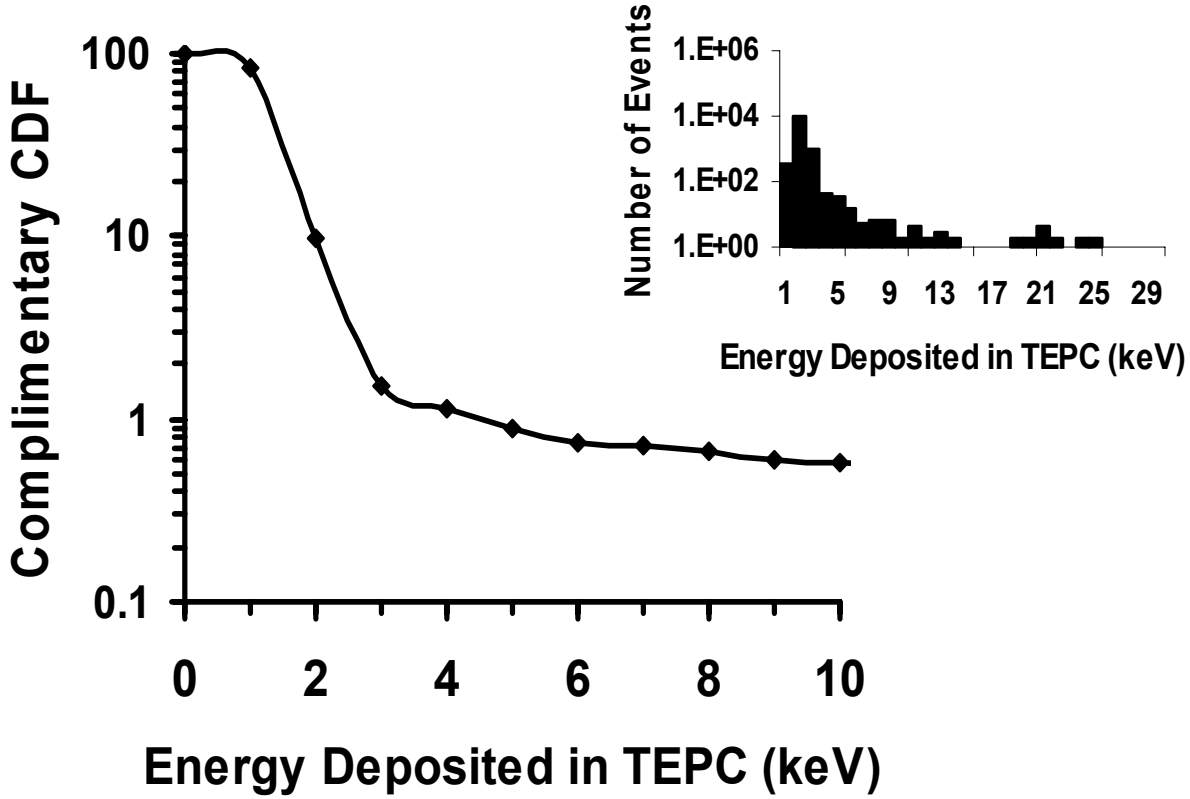
Complimentary CDF
100
10
1
0.1
0
2
4
6
8
10
Energy Deposited in TEPC (keV)
Number of Events
1.E+06
1.E+04
1.E+02
1.E+00
1
5
9
13
17
21
25
29
Energy Deposited in TEPC (keV)

Figure 2

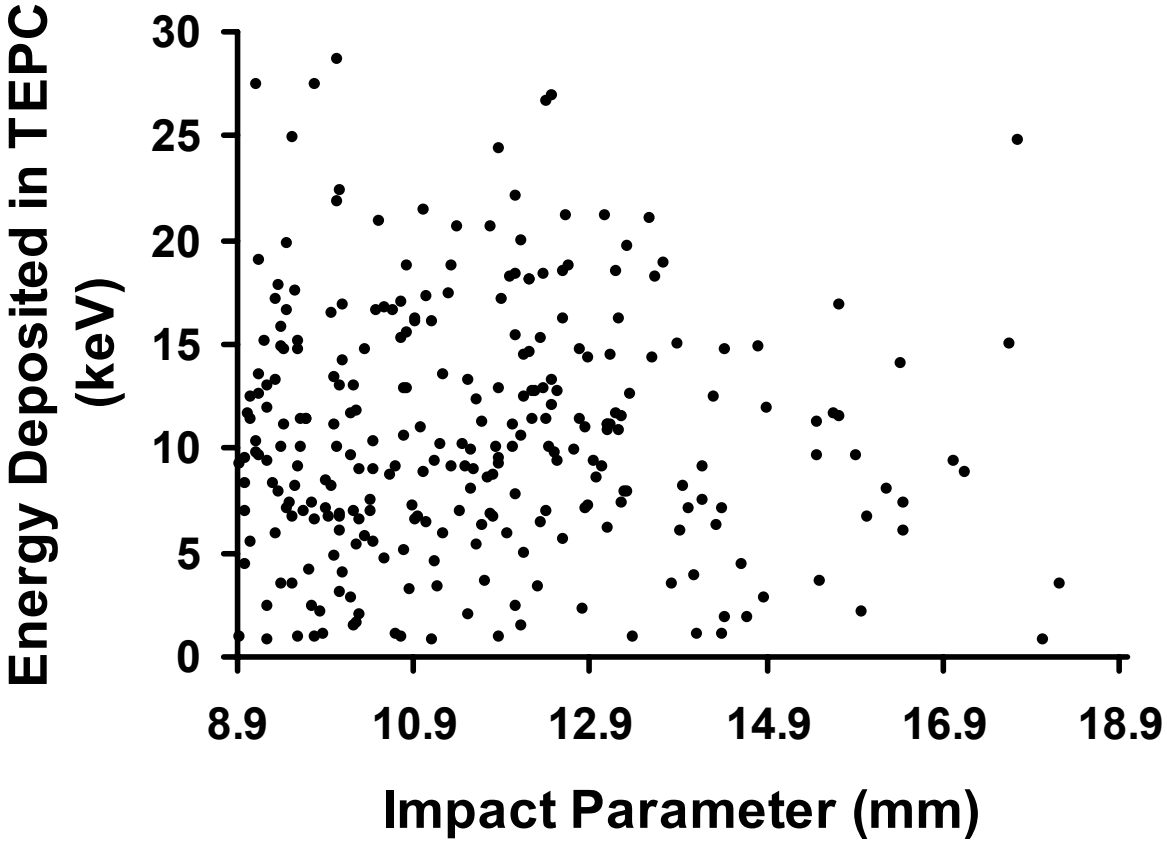
Energy Deposited in TEPC (keV)
30
25
20
15
10
5
0
8.9
10.9
12.9
14.9
16.9
18.9
Impact Parameter (mm)

Figure 3

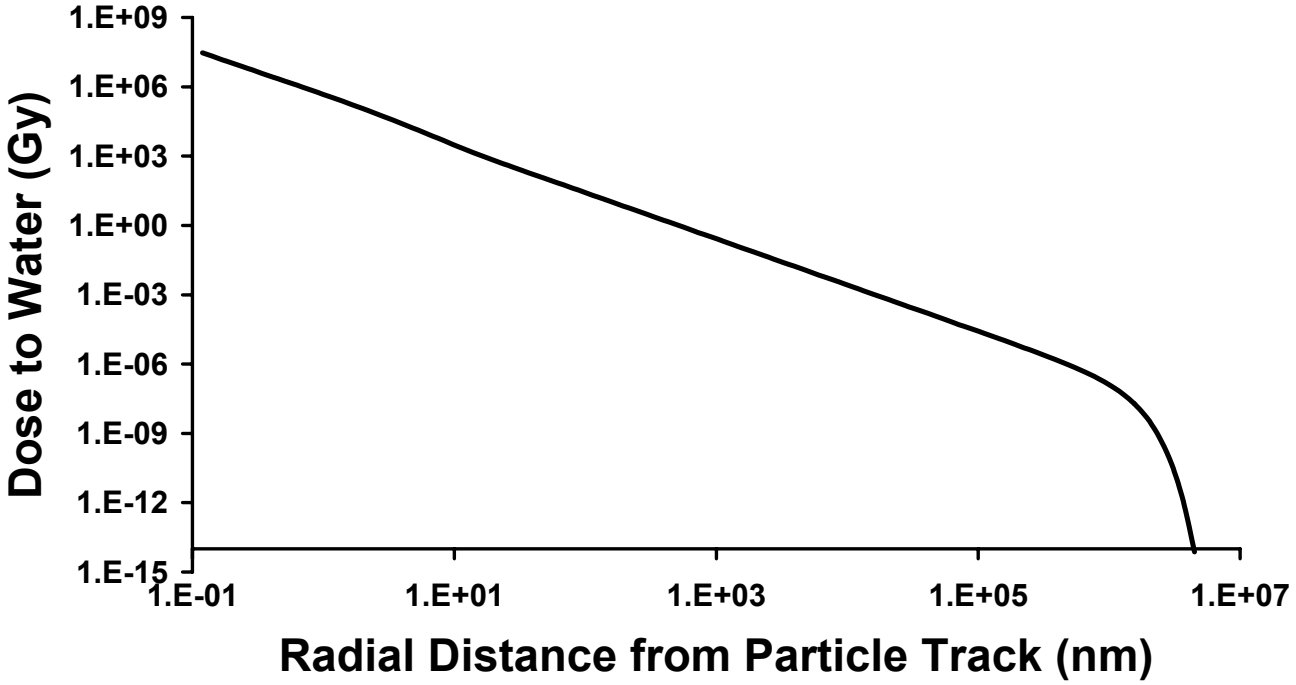
1.E+09
1.E+06
1.E+03
1.E+00
1.E-03
1.E-06
1.E-09
1.E-12
1.E-15
Dose to Water (Gy)
1.E-01
1.E+01
1.E+03
1.E+05
1.E+07
Radial Distance from Particle Track (nm)

Figure 4

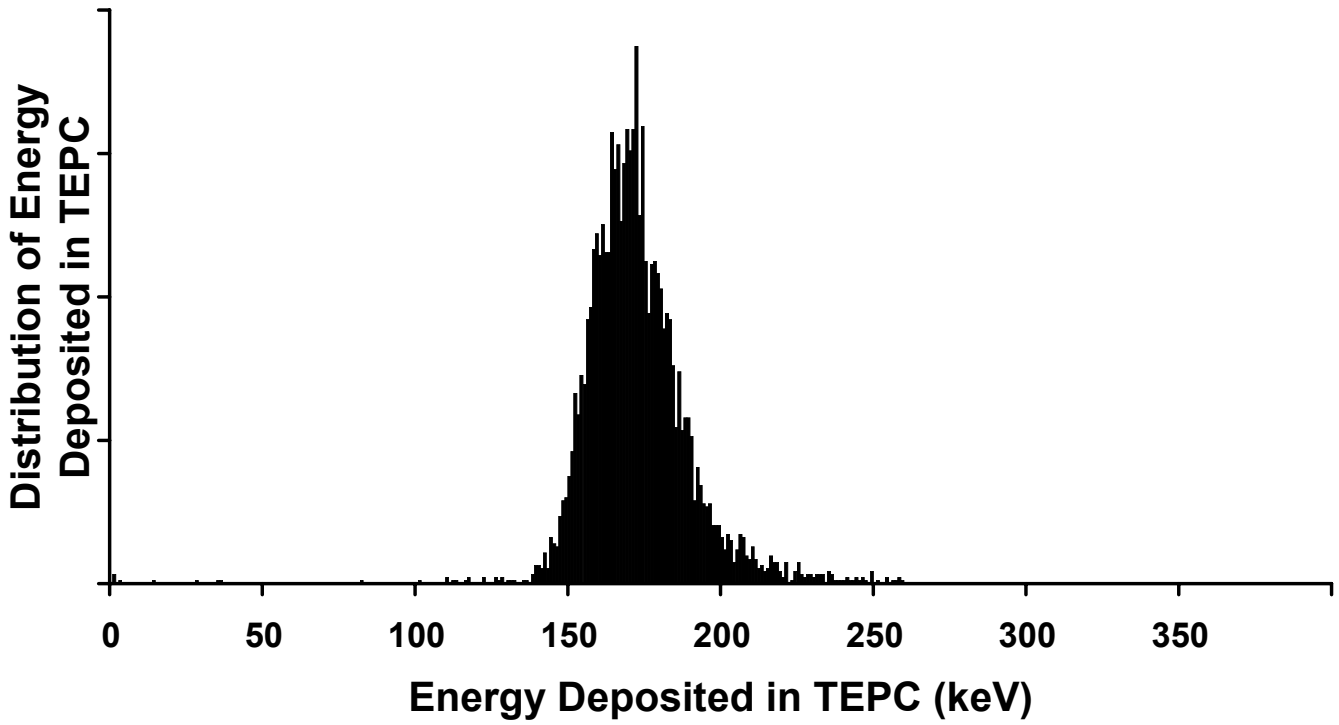
Distribution of Energy Deposited in TEPC
0
50
100
150
200
250
300
350
Energy Deposited in TEPC (keV)

Figure 5

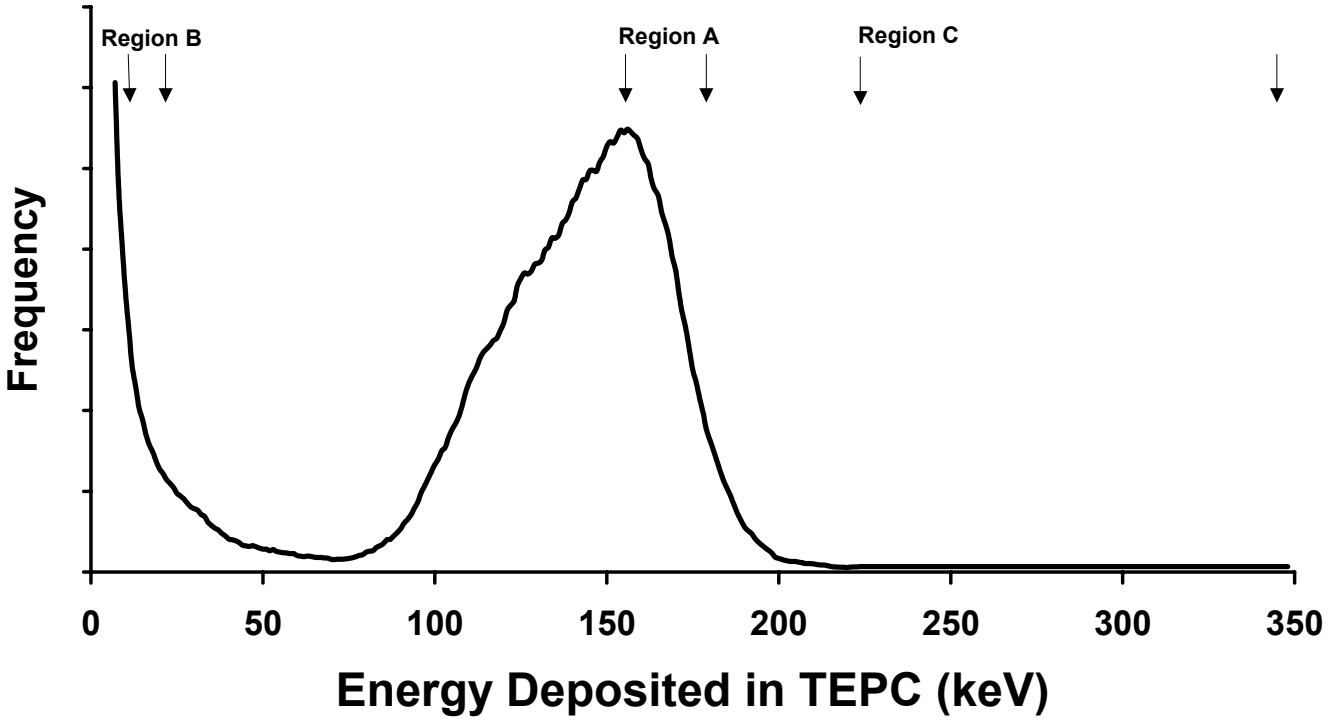
Region B
Region A
Region C
Frequency
0
50
100
150
200
250
300
350
Energy Deposited in TEPC (keV)

Figure 6

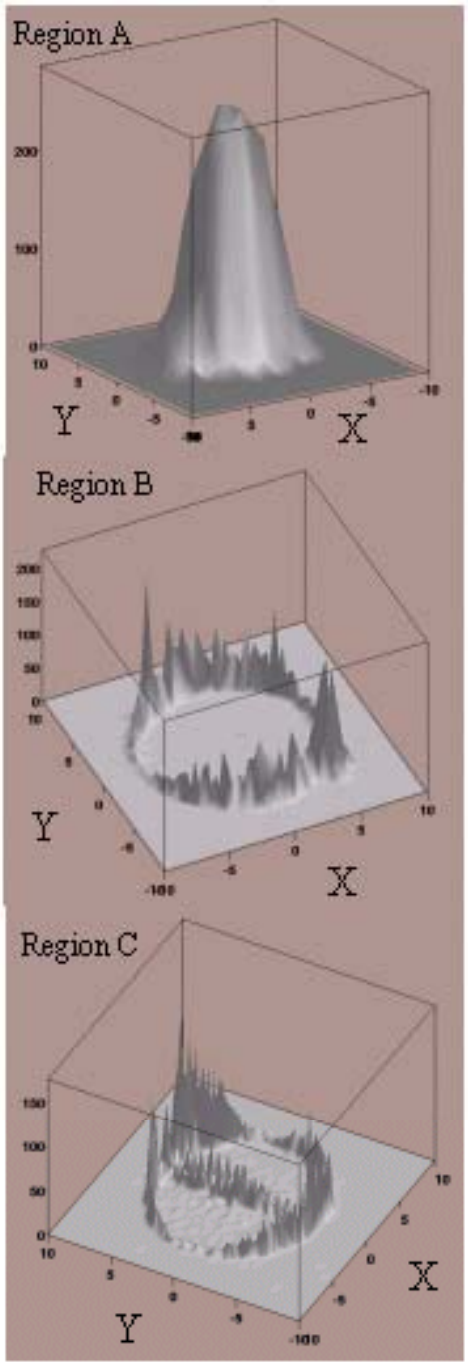

Figure 7

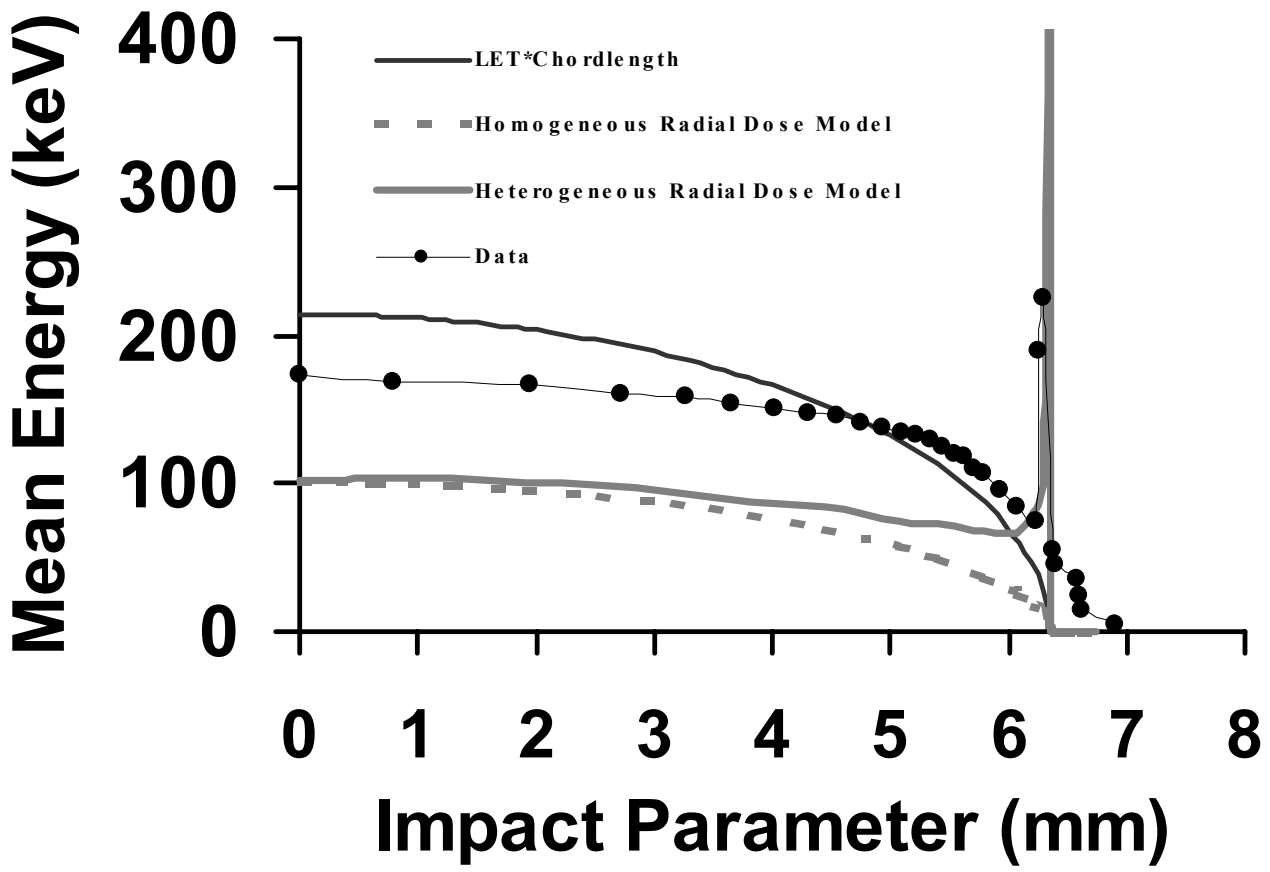
Mean Energy (keV)
400
300
200
100
0
LET*Chordlength
Homogeneous Radial Dose Model
Heterogeneous Radial Dose Model
Data
0
1
2
3
4
5
6
7
8
Impact Parameter (mm)

Figure 8

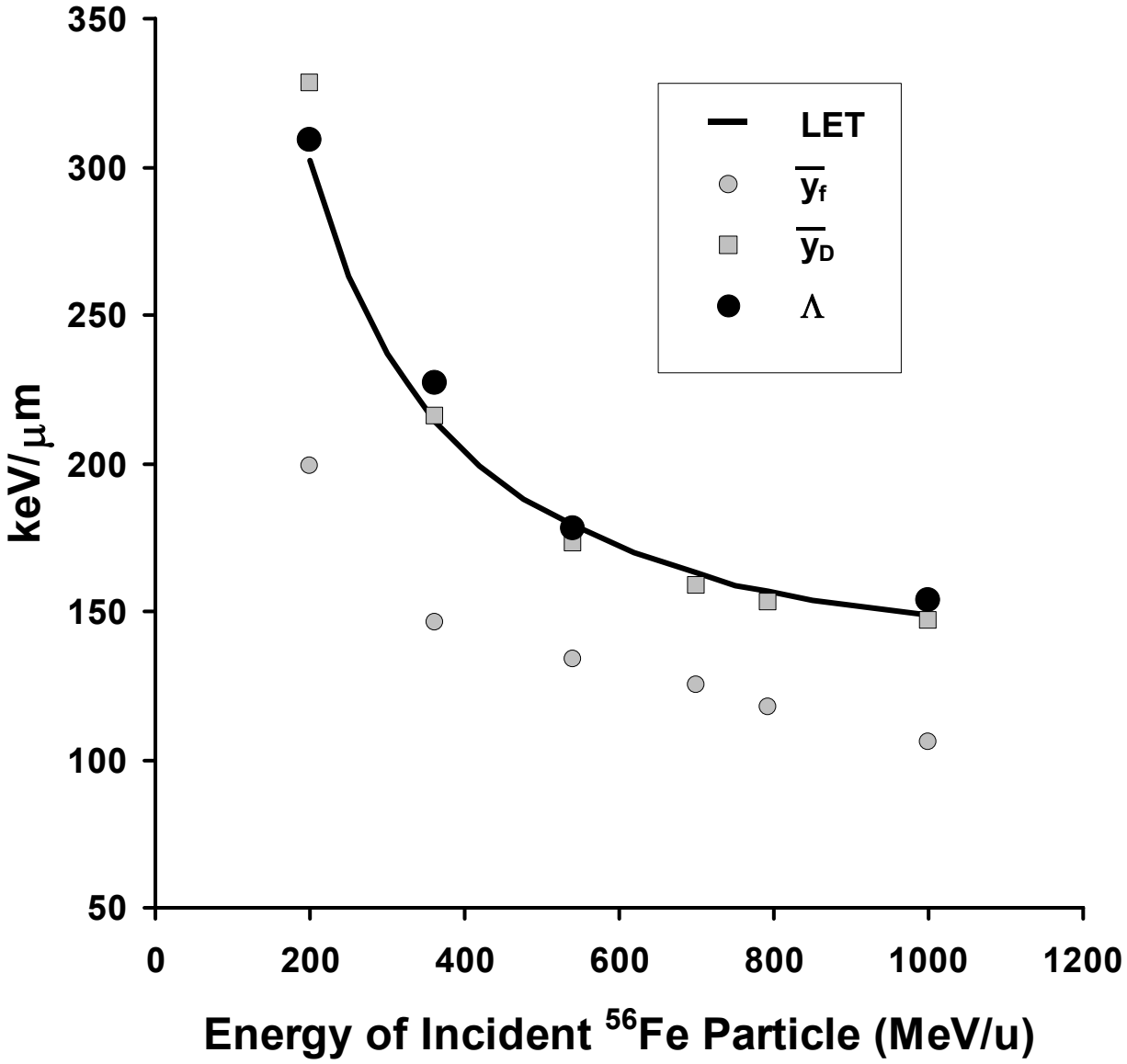
350
300
250
200
150
100
50
keV/μm
0
200
400
600
800
1000
1200
Energy of Incident 56Fe Particle (MeV/u)
LET
$\overline{y_f}$
$\overline{y_D}$
Λ

Figure 9

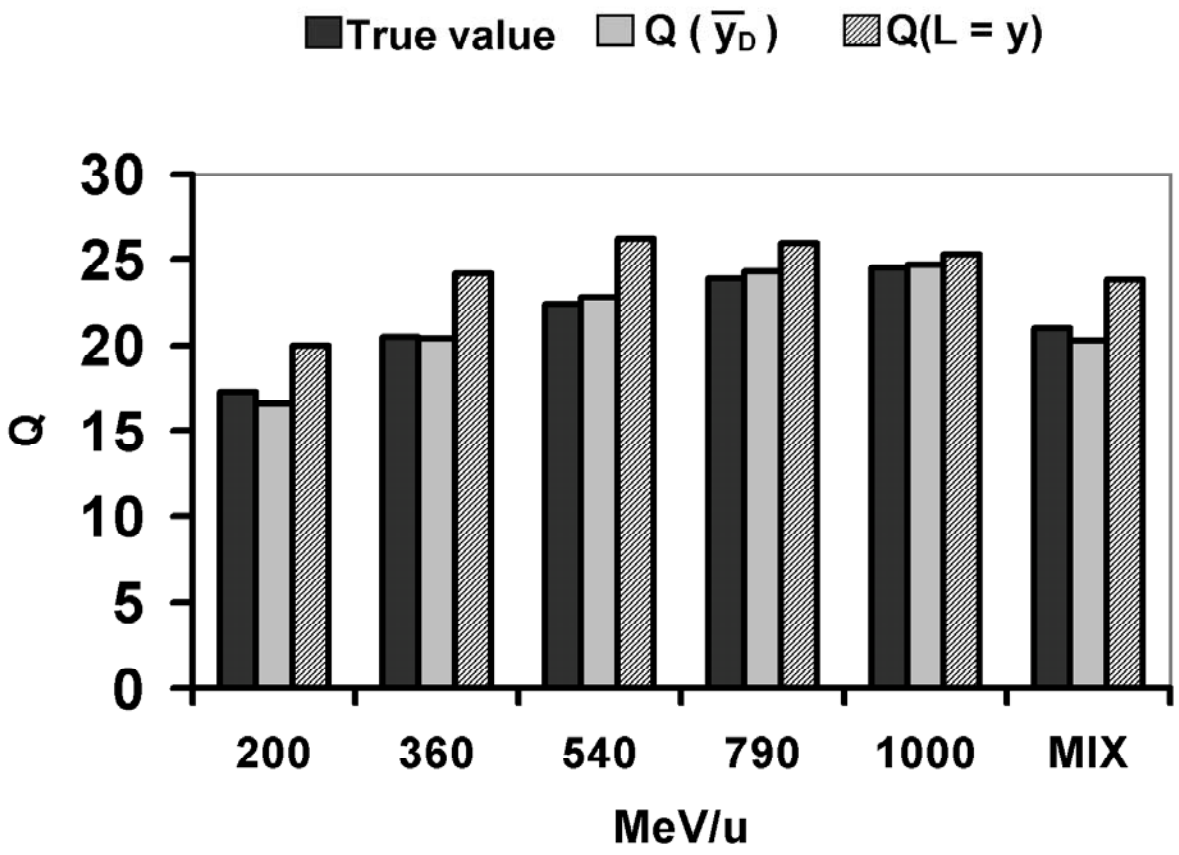
True value
Q ($\overline{y}_D$)
Q(L = y)
30
25
20
15
10
5
0
Q
200
360
540
790
1000
MIX
MeV/u

Figure 10